

Experimental study of the suppression of Rayleigh–Bénard instability in a cylinder by combined rotating and static magnetic fields

Ilmārs Grants¹, Alexander Pedchenko², Gunter Gerbeth¹

¹ Forschungszentrum Rossendorf, MHD Dept., P.O. Box 510119, 01314 Dresden, Germany

² Institute of Physics, University of Latvia, LV-2169 Salaspils, Latvia

Abstract. We consider experimentally transition in a liquid metal cylinder heated from below and subject to superimposed rotating and static magnetic fields. Being itself unstable, a strong enough rotating magnetic field driven flow suppresses considerably the temperature fluctuations due to the thermo-gravitational convection. The superimposed static ‘cusp’ magnetic field reduces further the amplitude and characteristic period of remaining temperature fluctuations while a superimposed uniform axial field has no such effect. This behavior agrees quantitatively with the differing effects of both static fields on the additional unstable Taylor vortex type solutions, which bifurcate sub-critically and actually govern the transition in the rotating magnetic field driven flow. Thus, the observations are consistent with the description of a turbulent shear flow as a trajectory wound irregularly on the skeleton of the additional unstable flow states. If this ‘skeleton’ is compressed by an external influence (the ‘cusp’ static field in our case), then also the averaged amplitude of turbulent fluctuations decreases by the same factor.

1. Introduction

The problem under consideration stems from the crystal growth technologies where inverse thermal gradients are often met, and the occurrence of flow oscillations is usually to be avoided. The inherently unstable configuration of a liquid heated from below can be stabilized by mechanical rotation [1]. This effect is traditionally used in crystal growth technologies. If the liquid is a good electrical conductor (and semiconductor melts are) then the rotation can also be forced magnetically by a rotating magnetic field [2]. A steady magnetic field also stabilizes a liquid heated from below [1, 3, 4, 5]. It turns out, however, that the stabilization by an RMF is energetically much more effective since the required field flux density is much lower compared to a steady magnetic field [6, 7]. The stabilizing capability of a rotating magnetic field (RMF) is limited by the hydrodynamical Taylor–Görtler instability powered by the outwards decreasing radial profile of the angular velocity near the side wall [7]. A superimposed steady magnetic field suppresses this instability [8]. As a result, a combination of rotating and steady magnetic fields is able to stabilize the flow considerably more than both fields separately — the field effects ‘multiply’. The Rayleigh number may be still too large in real crystal growth applications to fully stabilize the melt motion by the combined magnetic fields. Even so, they may be used to damp the turbulent temperature fluctuations. It has been shown [7] that a sufficiently strong RMF reduces the amplitude of temperature fluctuations considerably if the magnetic forcing outweighs buoyancy. This may be regarded as an ‘embedded transition’ between a large scale,

large amplitude buoyancy and a small scale, small amplitude RMF driven flow turbulence. The later state is largely controlled by Taylor vortex type structures represented by the additional unstable steady solutions [8]. These solutions bifurcate sub-critically well below the first linear instability of a different kind [9] and control actually the nonlinear transition of the RMF driven flow in the presence of tiny imperfections [10]. This transition has much in common with the sub-critical transition in shear flows although the mechanisms are different. Namely, a slightly disturbed linearly stable RMF driven flow may become turbulent similarly as it is observed, for instance, in the pipe flow. According to the description of Grossmann [11] the properties of the irregular (or turbulent) motion under the nonlinear transition are closely related to the properties of sub-critical coherent structures, particularly, the additional unstable steady solutions. The motion is imagined as a trajectory wound irregularly on a skeleton of those coherent structures. Thus, knowing the effect of some control parameter on the amplitude of the additional solutions, one can estimate the effect of this parameter on the amplitude of the fluctuations.

The amplitude of the additional steady solutions in an RMF driven flow decreases considerably if a static ‘cusp’ magnetic field is superimposed [8]. Thus, one may expect that a combination of RMF and steady ‘cusp’ field will damp the flow fluctuations more efficiently than the RMF alone. That was indeed supported by a few runs of a direct numerical simulation (DNS) [8]. Consequences of these observations still remain rather uncertain since it is impossible to know for sure all the additional solutions, either steady or periodic. Besides, the DNS results are so far too fragmentary and may also be dependent on the nature of the numerical imperfections that, in turn, may differ essentially from the natural ones.

The main purpose of our study is to widen the knowledge about the ‘embedded transition’ in the magnetically driven rotating flow heated from below, and to investigate the possibilities of prediction of related phenomena in general. We focus our study mainly on two questions: (i) Are the conclusions upon the additional unstable steady solutions confirmed experimentally? (ii) What are other properties of the magnetically forced turbulent flow?

2. Problem formulation

The experiment was designed to approximate the conditions of our previous numerical study [8]: (i) isothermal top and bottom; (ii) adiabatic side wall; (iii) low-frequency, low induction rotating magnetic field; (iv) electrically insulating walls. The low-frequency, low induction condition implies that the RMF experiences no skin effect and rotates much faster than the flow it induces. The superimposed static magnetic field was either axial uniform or the so-called ‘cusp’ field in this study.

Liquid Gallium was chosen as working liquid since it is a metal with second lower melting temperature next to Mercury and unlike the latter has much less security constrains. Gallium was also used in previous experimental studies [6, 7, 12].

Table 1. The governing dimensionless parameters

parameter	symbol	definition	value or range
Aspect ratio	R	R_o/H_o	1.0
Prandtl number	Pr	ν/κ	0.0285
Grashof number	Gr	$\beta g T' H_o^4/\nu^2$	$[0.2:6] \times 10^6$
Magnetic Taylor number	Ta	$\sigma \omega_o B_o^2 H_o^4/2\rho\nu^2$	$[0.1:30] \times 10^6$
Hartmann number	Ha	$(\sigma/\rho\nu)^{1/2} B H_o$	105 or 0

The problem is defined by five governing parameters, see Table 1. Symbols ν , κ , β , ρ and σ denote here the kinematic viscosity, temperature diffusivity, thermal expansion, density and electric conductivity of liquid Gallium, respectively, with average values $\nu = 3.19 \times 10^{-7} \text{ m}^2/\text{s}$, $\kappa = 1.12 \times 10^{-5} \text{ m}^2/\text{s}$, $\beta = 1.02 \times 10^{-4} \text{ 1/K}$, $\rho = 6.067 \times 10^3 \text{ kg/m}^3$ and $\sigma = 3.82 \times 10^6 \text{ S/m}$ taken from Ref. [12]. The RMF frequency and amplitude of the flux density is denoted by ω_o and B_o , respectively. The scale of the static field is denoted by B . In case of the ‘cusp’ field, this scale is equal to the maximum value of the axial field component at the axis of the cylinder: $\mathbf{B} = B(-0.5r/H_o\mathbf{e}_r + z/H_o\mathbf{e}_z)$. The height of the cylinder $2H_o$ was equal to the diameter $2R_o = 60 \text{ mm}$ in this study. This size allows to exceed the critical Grashof number of the purely thermal case by a factor of 700 when the mean temperature gradient T' is at the maximum (around 7.5 K/cm).

3. Setup and measurement technique

3.1. Cell

The container of height equal to diameter of 60 mm was made of a polished Plexiglass tube and two copper covers (Figure 1). Each cover was made of two 12 mm thick copper discs both of which had two 6×8 mm cross-section circular channels for heating/cooling water. The mean diameters of the channels were 22 and 44 mm, respectively. The upper cover had a 3 mm diameter hole through the center for filling purposes. The internal surface of covers was polished and painted with an electrically insulating paint to avoid electrical contact with Gallium. The outer surfaces of the cell and copper discs were covered with heat insulating material to prevent heat losses to the environment.

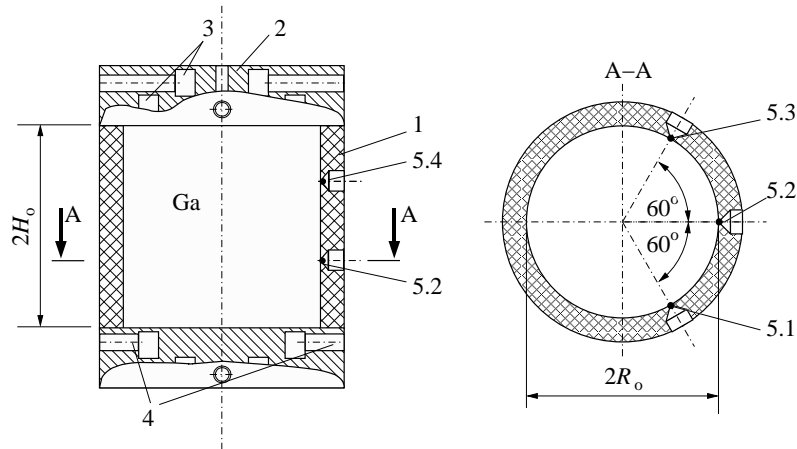


Figure 1. Scheme of container; 1 — Plexiglass cylinder; 2 — copper covers; 3 — circular channels; 4 — water inlets; 5.1–5.4 — thermistors.

3.2. Magnetic fields

Three type of magnetic fields were used in this experiment: rotating, steady axial, and steady ‘cusp’ fields. The rotating magnetic field was generated by a six coil inductor in one pole pair connection. Maximum flux density was 2.6 mT, frequency was 30 Hz, which corresponds to a shielding factor of $K = \sigma\mu_o\omega R_o^2 = 0.81$. The field non-uniformity in the control volume was less than 1.2%. The steady axial magnetic field was produced by a solenoid of dimensions exceeding the cell size in more than 10 times. The non-uniformity of the steady field was less than 1% in the experimental volume. The axial field strength was $B = 80 \text{ mT}$.

A system of permanent NdFeB ring magnets was used for the ‘cusp’ field. Each pole piece was composed of four $76 \times 42 \times 6$ mm (outer diameter, bore diameter, thickness), four $40 \times 23 \times 6$ mm and four $20 \times 0 \times 5$ mm magnets. Distance between the opposite poles was 120 mm. The resulting maximum axial field flux density near the internal surface of the container cover was $B = 80$ mT.

3.3. Temperature measurement

Four 0.3 mm diameter glass encapsulated miniature thermistors (YSI Corp./32A48) were installed in 1 mm diameter holes in the container side wall with their tips aligned with the internal surface of the container (Figure 1). Three of them were placed at the height of 20 mm above the bottom cover with 60 degrees angular displacement along the azimuth. The fourth thermistor was placed 20 mm below the top cover opposite to the middle of three lower sensors.

The signals from the thermistors were simultaneously registered by four Keythley K2000 multimeters. Thermistors were fed by a small DC current of $10 \mu\text{A}$ provided by the multimeter, thus, limiting the self-heating effect of the thermistor. All four thermistors were calibrated individually. The thermistor sensitivity changed from ≈ 50 Ohm/K at $T = 303$ K to ≈ 10 Ohm/K at $T = 333$ K. The error of the temperature measurements increased with the temperature and was between 0.001 and 0.005 K, respectively.

The cooling/heating water was supplied at a flow-rate of about 3 l/min from the baths of two thermostats. Temperature in both thermostat baths was controlled within 0.1 K tolerance by two temperature probes (pt1000) installed on the outer surface of the cell covers. The applied temperature difference divides between the copper covers, their electric insulation and the Gallium bulk. To measure the part which applies directly to the Gallium bulk we performed the following test. A stable temperature gradient was applied by setting the temperature difference of the thermostats to $\Delta T = 12$ K. The temperature difference between the vertically displaced (by 2 cm) thermistors was measured to be 3.50 K that corresponds to $T' = 3.5/2 = 1.75$ K/cm or $T' = 7/8 \Delta T / 2H_o$. This expression of the temperature gradient was used in the Grashof number definition (Table 1) further on.

4. Results

We considered four cases with $\Delta T = 12, 18, 30$ and 50 K (the Grashof number 1.4, 2.1, 3.5 and 5.8×10^6 , respectively). The standard deviation of the temperature variation is plotted versus the strength of the rotating field in Figure 2. Transition under both the superimposed axial and ‘cusp’ steady fields was considered as well as the case of RMF alone for $\Delta T = 30$ and 50 K. The amplitude of temperature fluctuations went down by a factor of 10 to 30 during the transition. In all cases we observed a more pronounced transition for a superimposed ‘cusp’ field compared to the axial field case, particularly for higher ΔT . The strongest suppression of fluctuations was with the ‘cusp’ field shortly after the transition. The corresponding threshold value of the Taylor number vs. the Grashof number is shown as inset of Figure 2. This dependency was well approximated by a power function with an exponent of 0.8.

Figure 3 shows correlations of signals from thermistors 2 and 4 symmetrically placed on opposite sides of the mid-plane $c_{24}(0)$ according to the definition

$$c_{ij}(\tau) = c_{ij}(\Delta n \Delta t) = \sum_{n=1}^{N-\Delta n} \frac{u_i(t_n)u_j(t_n + \tau)}{\left(\overline{u_i^2} \overline{u_j^2}\right)^{1/2}}, \text{ where } u_i(t_n) = T_i(t_n) - \bar{T}_i.$$

Symbols N and Δt denote the total number of time layers and the time step, respectively. The fluctuations remained vertically correlated well above the transition in case of the superimposed steady axial field. Otherwise, the vertical correlation disappeared immediately after the transition.

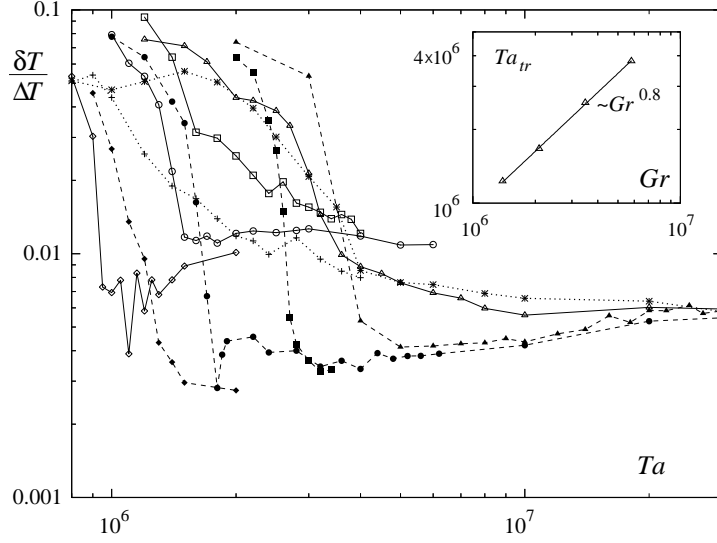


Figure 2. The mean standard deviation of temperature fluctuations vs. the magnetic Taylor number. Diamonds, circles, boxes and triangles display $\Delta T = 12, 18, 30$ and 50K cases while filled and open symbols correspond to ‘cusp’ and axial field, respectively. Crosses and asterisks refer to the no steady field case with $\Delta T = 30$ and 50K , respectively. The inset shows the dependency of the transitional Taylor number vs. the Grashof number.

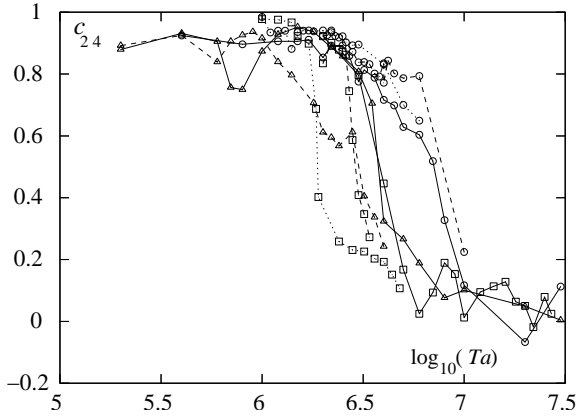


Figure 3. Correlation of signals from vertically displaced sensors vs. the magnetic forcing. Boxes, circles and triangles refer to the ‘cusp’, axial and no steady field cases, respectively. Solid dashed and dotted lines correspond to $\Delta T = 50, 30$ and 18K , respectively.

The instantaneous azimuthal correlation, in turn, continued to increase with Ta after the transition for all field configurations (Figure 4). The azimuthal correlation stayed comparably low in case of the ‘cusp’ field. Pronounced minimums were observed for RMF alone or with the steady axial field due to the temporary change from the azimuthal wavenumber $m = 1$ to a $m = 2$ mode dominated regime. The azimuthal correlation of time-shifted signals was higher. Its maximum approached unity just before the transition at $Ta = 3 \times 10^6$ for $\Delta T = 50$ for all field configurations and declined afterwards (Figure 4). The time delay at which the maximum azimuthal correlation is reached can be associated with the angular velocity of thermal structures transported by the rotating flow. This velocity

$$\omega_{\text{cor}} = \frac{\Delta\phi_{ij}}{\tau_{\text{max}}^{ij}}, \quad \text{where } \tau_{\text{max}}^{ij} \text{ is defined by } c_{ij}(\tau_{\text{max}}^{ij}) = \max_{\tau} c_{ij}(\tau),$$

is shown versus the forcing in Figure 5.

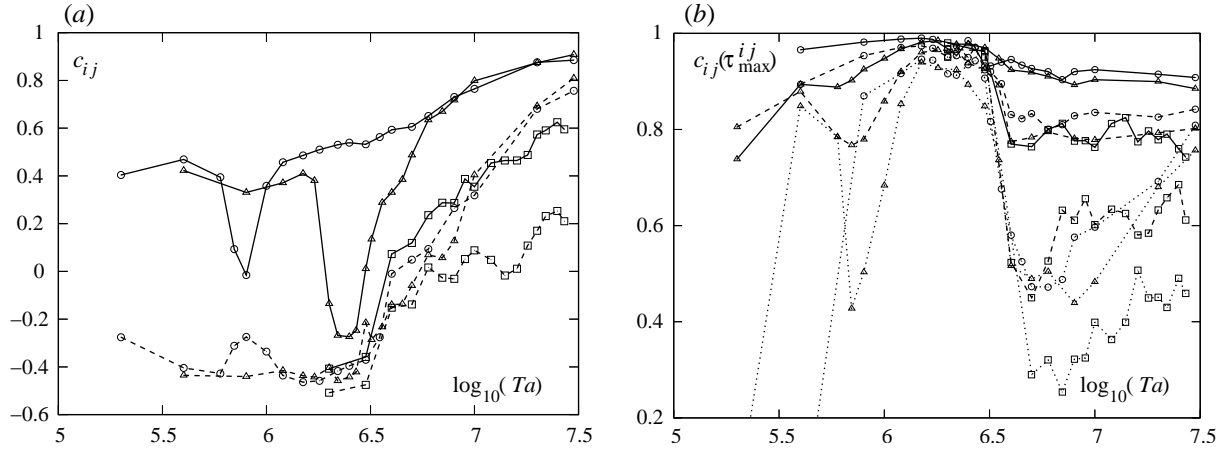


Figure 4. The azimuthal correlation vs. the magnetic forcing at $\Delta T=50\text{K}$: (a) Instantaneous correlation, (b) correlation of time shifted signals maximized by the shift delay. Solid, dashed and dotted lines correspond to correlations of signals from sensors displaced by $\pi/3$, $2\pi/3$ and $4\pi/3$ in the flow direction, respectively. The ‘cusp’, axial and no steady field cases are displayed by boxes, circles and triangles, respectively.

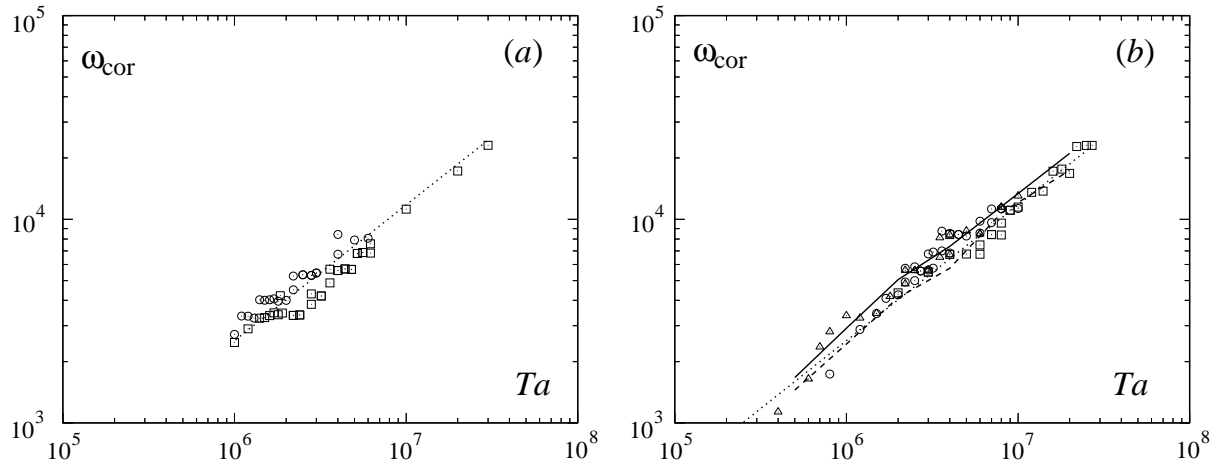


Figure 5. The dimensionless angular velocity of rotating thermal structures vs. the magnetic forcing: (a) $\Delta T = 18\text{K}$, (b) $\Delta T = 50\text{K}$. Boxes, circles and triangles correspond to ‘cusp’, axial and no steady field cases, respectively. The angular velocity is expressed as the angular displacement of thermistors divided by the time of delay to reach the maximum correlation. Thick solid and dashed lines display axisymmetric numerical results for the mean angular velocity under uniform axial and ‘cusp’ static field, respectively. The dotted line displays a $Ta^{2/3}$ slope.

Two typical cases of the fluctuation frequency power spectrum are shown in Figure 6. Pronounced low frequency peaks were observed in case of a superimposed axial field shortly after the transition. The high-frequency falloff was considerably more flat for the ‘cusp’ field.

5. Discussion and conclusions

Being itself unstable, the magnetically driven flow may considerably suppress the temperature fluctuations in a liquid heated from below when the forcing is raised above a certain threshold.

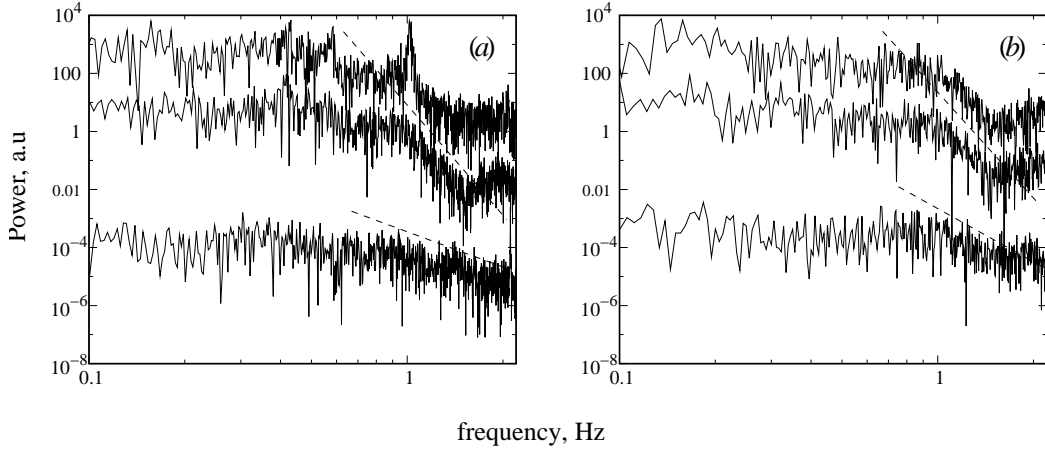


Figure 6. Frequency power spectrum of temperature fluctuations in the magnetic forcing dominated regime at $\Delta T = 50\text{K}$: (a) $Ta = 5 \times 10^6$, (b) $Ta = 2 \times 10^7$. Steady axial, no steady field and ‘cusp’ field cases are placed top to bottom, respectively.

This type of flow regime change was the main subject of our study. We considered the effect of a moderate strength superimposed static (either uniform axial or the so-called ‘cusp’) magnetic field on this transition. The transition was well pronounced in terms of the fluctuation amplitude under the superimposed static ‘cusp’ field. For other field configurations the fluctuation amplitude dependency smoothed out at $\Delta T \geq 30\text{K}$. In terms of the time-shifted maximum azimuthal correlation over long scales (figure 4b), however, the transition was equally observable independently on the static fields at the highest Gr considered. Hence, we may assume that the ‘cusp’ field just sharpens the transition diagram in terms of the fluctuation amplitude while the transition in terms of the structure change is not much influenced by the static fields. Taking, thus, the ‘cusp’ field as a representative case and defining the transitional magnetic forcing as intersection $\delta T(Ta_{tr}, Gr)/\Delta T = 0.01$ we obtained the estimate $Ta_{tr}(Gr) = O(Gr^{4/5})$. Alternatively, the ‘critical’ Grashof number was $Gr_c = O(Ta^{5/4})$. Expressed in terms of the core angular velocity Ω (for which the $Ta^{2/3}$ scaling was observed, see figure 5) this relation is $Gr_c = O(\Omega^{15/8})$. This exceeds considerably the threshold value in case of pure rotation $Gr_c = O(\Omega^{4/3})$ (Chandrasekhar 1961). Seemingly, the stabilizing action of the RMF is not restricted to the rotation it induces. A possible explanation may include the meridional flow: To cause instability the buoyancy forces $O(Gr)$ should reach the scale of the centrifugal forces $O(\Omega^2) = O(Ta^{4/3})$ driving the secondary flow in the horizontal boundary layers. Equalizing both quantities at Ta_{tr} , one has $Ta_{tr}(Gr) = O(Gr^{3/4})$ which is indistinguishable close to the observed scaling 0.8. If this scaling holds for higher control parameter values, then it may have an implementation for large semiconductor crystal growth techniques where the intrinsic Grashof numbers are in the order of 10^9 . One of the purposes of the mechanical rotation applied in such processes is the damping of the buoyancy driven fluctuations. Extrapolating the current results one may expect a difference between the magnetically and mechanically driven stabilizing angular velocity to grow by a factor of $O(Gr^{1/4})$.

One of the central questions of the current study concerns the amplitude of the temperature fluctuations in the RMF governed regime. According to the existing knowledge [14, 8] the turbulence arises from the Taylor-Görtler instability in the side layer. This instability is somewhat hidden by its non-linear appearance. Namely, the steady axisymmetric Taylor vortex type solutions remain disconnected from the basic state well above the first linear instability of a different type [9]. Our previous numerical study [8] showed that the amplitude of the

axisymmetric Taylor vortex steady additional solutions decreases by a factor of four when a static ‘cusp’ field with $Ha = 100$ is superimposed. Thus, one may expect a decrease of the amplitude of the temperature fluctuations according to the description of the excited state by Grossmann [11]. Such a decrease was indeed observed in our experiment in a regime shortly after the transition. The effect was particularly expressed at lower thermal gradients when a factor of four was observed in a perfect agreement with the predictions upon the amplitude of the additional solutions. Two consequences follow from these observations: (i) The application of combined RMF and static ‘cusp’ fields may be practically beneficial if the amplitude of the temperature fluctuations matters. (ii) Certain turbulence properties may be predicted from a numerical study of the additional flow solutions. Besides the fluctuation amplitude, the different static magnetic fields also act differently on other turbulence properties. In case of the superimposed static ‘cusp’ field the frequency spectra has a comparably flat falloff at high frequencies that means a larger share of small scale fluctuations. Consequently, both the amplitude and the characteristic scale of the turbulence near the side wall decreases in the ‘cusp’ field. The uniform axial field, in turn, may cause distinct frequency peaks just after the transition (figure 6). Different was also the effect of various field combinations on the correlation of signals from vertically displaced sensors. In case of the uniform static field, the vertical correlation persisted well above the transition and declined at $Ta = 10^7$ independently on the thermal gradient. The vertical correlation is due to large scale thermal waves, which dominate the unsteady flow below the transition. The thermal waves seem to be gradually replaced by steady field aligned structures after the transition. These structures break up as the forcing is further increased. No signs of such vertical structures were observed under the influence of the ‘cusp’ field. Unlike the vertical correlation the azimuthal one increases with the RMF strength for $Ta > Ta_{tr}$ under either combination of magnetic fields considered. This effect suggests the formation of a ‘quasi-axisymmetric’ turbulence, a regime dominated by circumferentially elongated structures near the side wall.

Acknowledgements

Financial support from German “Deutsche Forschungsgemeinschaft” in frame of the Collaborative Research Center SFB 609 is gratefully acknowledged. We acknowledge support from the European Commission under grant No. G1MA-CT-2002-04046.

- [1] Chandrasekhar S 1961 *Hydrodynamic and Hydromagnetic Stability* (Clarendon)
- [2] Moffatt H K 1965 *J. Fluid Mech.* **22** 521
- [3] Touihri R, Ben Hadid H and Henry D 1999 *Phys. Fluids* **11** 2078
- [4] Touihri R, Ben Hadid H and Henry D 1999 *Phys. Fluids* **11** 2089
- [5] Houchens B C, Martin Witkowski L, Walker J S 2002 *J. Fluid Mech.* **469** 189
- [6] Dold P and Benz K W 1995 *Cryst. Res. Technol.* **30** 1135
- [7] Friedrich J, Lee Y-S, Fischer B, Kupfer C, Vizman D, Müller G, 1999 *Phys. Fluids* **11** 853
- [8] Grants I and Gerbeth G 2004 *Phys. Fluids* **16** 2088
- [9] Grants I and Gerbeth G 2002 *J. Fluid Mech.* **463** 229
- [10] Grants I and Gerbeth G 2003 *Phys. Fluids* **15** 2803
- [11] Grossmann S 2000 *Rev. Mod. Phys.* **72** 603
- [12] M. P. Volz and K. Mazuruk K 2001 *J. Fluid Mech.* **444** 79
- [13] Grants I and Gerbeth G 2000 *J. Fluid Mech.* **431** 407
- [14] Kaiser Th and Benz K 1998 *Phys. Fluids* **10** 1104